

# Accurate Dynamic Modeling of Helical Ionic Polymer-Metal Composite Actuator Based on Intrinsic Equations

Hossein Moeinkhah, Jalil Rezaeepazhand, Alireza Akbarzadeh, and Il-Kwon Oh

**Abstract**—This paper presents dynamic modeling of an innovative contractible ionic polymer-metal composites (IPMC) actuator with a helical configuration. The helical shaped IPMC actuator is fabricated through the thermal treatment of an IPMC strip, which is helically coiled on a glass rod. This type of a soft actuator can be used to realize not only bending motion but also torsional and longitudinal motion. For the first time, an explicit analytical expression is developed for the computation of mode shapes and dynamic responses of a helical IPMC actuator based on the intrinsic equations of the naturally curved and twisted beam. The numerical transfer-matrix method is used to solve the systems of 12 linear ordinary differential equations with boundary conditions. In particular, the effect of the structural parameters on the performance of the helical IPMC actuator is evaluated, using experimental results and an analytical model. The validation of the proposed model is achieved through comparison with computational results using a commercial finite-element (FE) program as well as experimental results. The present experimental and theoretical results show that diameter, among the structural parameters, plays an important role in the actuation performance of a helical IPMC actuator. The proposed modeling is general and can also be used in solving other cylindrical or noncylindrical helical IPMC actuators with different cross-sectional shapes as well as various end conditions.

**Index Terms**—Analytical model, circuit, distributed RC line, helical actuator, ionic polymer-metal composite (IPMC).

## I. INTRODUCTION

RECENTLY, the trend of new actuator applications has led researchers to develop novel actuation materials, which are light, compact, and driven by low power. Ionic polymer-metal composites (IPMCs) are a new class of electro-active polymers (EAPs) that show large bending deformation under a

very low input voltage [1]. Because of such remarkable properties, IPMCs have a promising future for applications in different areas such as biomimetic actuator and sensor [2]–[6], industrial and biomedical devices [7], [8] and energy harvesters [9]–[13]. Up to now, numerous studies have been reported by many researchers for the fabricating [14], [15], modeling [16]–[22], simulation, and control [23]–[25] of the IPMC actuator that are used in novel devices for different applications.

Helix is one of the most fascinating curves in science and nature. Helical structures can be found in nanosprings, carbon nanotubes,  $\alpha$ -helices, DNA double and collagen triple helix [26], [27]. In the field of smart materials, especially a shape memory alloy (SMA), helices can be used to enhance the mechanical bandwidth and energy efficiency of the devices [28]. The SMA springs are important kind of actuators that are used in various kinds of applications. These actuators have attracted the attention of several authors. Han *et al.* [29] presented a SMA helical actuator that can be used to enhance buckling capacity of columns. The application of the SMA helical actuator in an active catheter medical device was demonstrated by Lee and Lee [30]. Li *et al.* [31] explored the application of a helical IPMC actuator as a radius control of biomedical active stents. They showed that the diameter of the helix plays an important role in improving the actuation performance. A helical-shaped IPMC actuator offers several advantages. Helix could be used for generating radial and longitudinal motion. Based on the actuation mechanism of the IPMC actuator, the helical IPMC actuator transforms the bending motion into the torsional and linear motion.

To the best of our knowledge, although experimental and numerical modeling of the helical shape IPMC actuator have been presented in the literature [31], [32], there is not any report on analytical dynamic modeling of the helical IPMC actuators. The necessity for new applications requiring a multi-DOF motion has motivated the authors to seek an analytical and numerical solution for helical type IPMC actuators. A detailed understanding of the behavior of a helical beam under dynamic conditions is crucial for the design of modern high-performance helical IPMC actuators. Therefore, it is the goal of this study to derive new analytical governing equations for a cylindrical helical IPMC actuator with rectangular cross section in the presence of the input voltage and the associated natural boundary conditions. To do this, an efficient method for analysis in the Laplace domain and differential geometry are used.

The remaining of this paper is organized as follows. In Section II, centerline geometry of a helical beam is derived based on

Manuscript received February 24, 2014; revised July 4, 2014; accepted August 1, 2014. Date of publication October 20, 2014; date of current version August 12, 2015. Recommended by Technical Editor F. Carpi. This work was supported by a National Research Foundation of Korea Grant funded by the Korean Government (2012R1A2A2A01047543). (Corresponding authors: Hossein Moeinkhah and Il-Kwon Oh).

H. Moeinkhah is with the Department of Mechanical Engineering, University of Sistan and Baluchestan, Zahedan, Iran and also with the Center of Excellence on Soft Computing and Intelligent Information Processing, SCIIP, Department of Mechanical Engineering, Ferdowsi University of Mashhad, Mashhad, Iran (e-mail: hmoein@gmail.com).

J. Rezaeepazhand and A. Akbarzadeh are with the Center of Excellence on Soft Computing and Intelligent Information Processing, SCIIP, Department of Mechanical Engineering, Ferdowsi University of Mashhad, Mashhad, Iran (e-mail: jrezaeep@um.ac.ir; ali\_akbarzadeh@um.ac.ir).

I.-K. Oh is with the Division of Ocean Systems Engineering, School of Mechanical, Aerospace and Systems Engineering, Korea Advanced Institute of Science and Technology, Daejeon 305-701, Korea (e-mail: ikoh@kaist.ac.kr).

Color versions of one or more of the figures in this paper are available online at <http://ieeexplore.ieee.org>.

Digital Object Identifier 10.1109/TMECH.2014.2347356

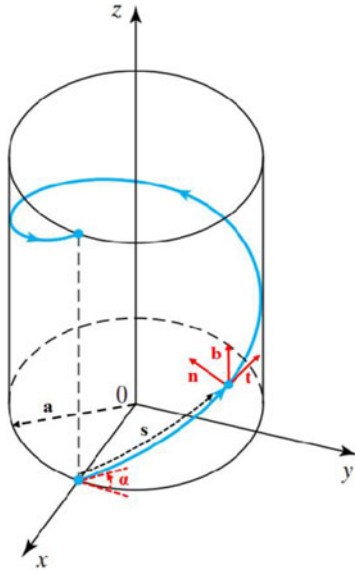


Fig. 1. Center line of the helical IPMC actuator.

the intrinsic equation of a helix. The electromechanical model of the helical IPMC actuator is derived in Section III. To explain the highly nonlinear dynamic responses of the helical IPMC actuator, the specific electromechanical model is newly formulated based on the naturally curved and twisted beam theory. In Section IV, the numerical transfer-matrix method is developed to solve the systems of 12 linear ordinary differential equations with boundary conditions using the fourth-order Runge–Kutta method. The effect of the structural parameters on the performance of the helical IPMC actuator is analyzed using experimental results and an analytical model. Finally, the verification of the results using a commercial FE package is presented in Sections V–VII. Concluding remarks are made in Section VIII.

## II. GEOMETRY OF THE HELICAL IPMC

From the view point of differential geometry, a cylindrical helix is a geometric curve with nonzero constant curvature  $\kappa$  and nonzero constant torsion  $\tau$ . A helical IPMC actuator is an IPMC beam with rectangular cross section having a helical curve as its centerline shown in Fig. 1. If  $s$  denotes the curvilinear coordinate along the helix centerline, the position vector of a point on the curve can be expressed as

$$\mathbf{r} = a \cos \beta \mathbf{i} + a \sin \beta \mathbf{j} + b \beta \mathbf{k} \quad (1)$$

where  $\beta$  is the helix angle,  $b$  is the step for unit angle of the helix, and  $a$  is the radius of the helix. The Frenet tangential ( $\mathbf{t}$ ), normal ( $\mathbf{n}$ ), and binormal ( $\mathbf{b}$ ) unit vectors associated with helix center line are

$$\mathbf{t} = \mathbf{r}' / \|\mathbf{r}'\|, \quad \mathbf{n} = \mathbf{r}\mathbf{t}' / \|\mathbf{r}\mathbf{t}'\|, \quad \mathbf{b} = \mathbf{t} \times \mathbf{n} \quad (2)$$

where superscript prime denotes the derivative with respect to the parameter  $s$ . The following differential relations among the unit vectors  $\mathbf{t}$ ,  $\mathbf{n}$ , and  $\mathbf{b}$  can be obtained based on the

Frenet–Serret formulae [33]

$$\begin{bmatrix} \mathbf{t} \\ \mathbf{n} \\ \mathbf{b} \end{bmatrix}' = \mathbf{N} \cdot \begin{bmatrix} \mathbf{t} \\ \mathbf{n} \\ \mathbf{b} \end{bmatrix}, \quad \mathbf{N} = \begin{pmatrix} 0 & \kappa & 0 \\ -\kappa & 0 & \tau \\ 0 & -\tau & 0 \end{pmatrix}. \quad (3)$$

The infinitesimal length element of the cylindrical helix is defined as

$$ds = cd\beta, \quad c = \sqrt{(a^2 + b^2)}, \quad b = a \tan \alpha \quad (4)$$

where  $\alpha$  is the pitch angle. For a helix with radius  $a$  and pitch angle  $\alpha$ , a movement  $ds$  results in a rotation,  $d\cos(\alpha)/a$ , about the axis of the helix. The components of this rotation about the tangential and binormal axes are the tortuosity  $\tau$  and curvature  $\kappa$ , which are, therefore, given by

$$\tau = (\sin \alpha \cos \alpha)/a = b/c^2, \quad \kappa = (\cos^2 \alpha)/a = a/c^2. \quad (5)$$

The relationship between the Frenet triad ( $\mathbf{t}$ ,  $\mathbf{n}$ ,  $\mathbf{b}$ ) and the fixed reference frame ( $\mathbf{i}$ ,  $\mathbf{j}$ ,  $\mathbf{k}$ ) is

$$\{\mathbf{X}\}_{tnb}^T = [\mathbf{B}]\{\mathbf{X}\}_{ijk}^T$$

$$\mathbf{B} = \begin{pmatrix} -(a/c) \sin \theta & (a/c) \cos \theta & b/c \\ -\cos \theta & -\sin \theta & 0 \\ (b/c) \sin \theta & -(b/c) \cos \theta & a/c \end{pmatrix}. \quad (6)$$

## III. ELECTROMECHANICAL MODELING

The complete dynamic model of the actuator is comprised of two parts, namely an electrical model and an electromechanical model. The electrical model is related to the input voltage and ion movement inside the IPMC actuator, while the electromechanical model describes the relation between input voltage and displacement field of the actuator.

### A. Derivation of Electrical Impedance Model

As the first step in deriving the actuation model of a helical IPMC actuator, we will develop the electrical impedance model. The more accurate models proposed thus far are physical models that consider the ion movement and electrochemical coupling equations [34]–[37]. Both material linearity and nonlinearity are incorporated in the formulated models. Therefore, the obtained partial differential equations are very complex and difficult to solve. To overcome this problem, we use a distributed *RC* electrical circuit with simpler equations and similar dynamic effects.

There are many reports in the literature about IPMC modeling based on an equivalent electrical circuit, where the voltage is correlated to the tip displacement by coupling electrical and mechanical parameters [16], [19], [38]. Since the characteristic dimension in the helical IPMC actuator is the boundary layer thickness, which is much smaller than the typical radius of curvature; we can use our pervious electrical model [16]. At the interface between the surface electrode and membrane, we can observe the composite layer of the metal and polymer. Thus, the double-layer capacitors are formed on the interfaces of two electrodes and the electrolyte. Actually these layers should be considered as more than a simple capacitance. Bao *et al.* [39]

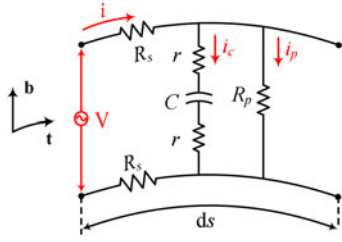


Fig. 2. Equivalent single unit circuit with current and voltage.

showed that simulation results of the clumped  $RC$  model cannot match the experimental data for an IPMC sample. They also claimed that the dendrite structure of the electrode causes nonlinearities and variation in capacitor values of the IPMC model. These effects were incorporated in the distributed model of the IPMC.

Since the applied voltage is small, the nonlinear effects of the complex impedances are neglecting in this study. The detailed analysis of nonlinear phenomena associated with large applied voltages was presented by Cha *et al.* [40]. The resulting linear distributed  $RC$  model, which is valid for small voltages, can be described by a series of similar circuits with discrete elements as illustrated in Fig. 2. In the present electrical model, the ion movement in the polymer membrane is modeled as double-layer capacitors in an equivalent circuit. The energy loss in the actuator is analogous to a resistance element in an electrical circuit. Also the stored electrical charge within the actuator is modeled as a capacitance element. The ionic polymer membrane that is permeated with water acts as an electric conductor and is modeled as a simple resistance in the electrical circuit.

In the case of helical IPMC actuator, the infinitesimal element is elongated in curvilinear coordinate direction  $s$  as shown in Fig. 2. Assume the electrode resistance per unit length is  $R_s$  in the  $\mathbf{t}$ -direction and  $r$  in the  $\mathbf{b}$ -direction for a single unit. The electrolyte between the electrodes introduces an internal resistance; which is represented by  $R_p$  as a shunt resistor between two electrodes in a single unit. The ion movement in polymer membrane can be modeled as double-layer capacitor  $C$  in an equivalent circuit. Voltage and current are assumed to be functions of the distance along the arc coordinate  $s$  and time  $t$ .  $i_c(s, t)$  is the distributed current per unit length flowing through the polymer due to the ion movement,  $i_p(s, t)$  represents the leaking current per unit length, and  $i(s, t)$  is the surface current on the electrodes. By defining  $z$  as Laplace variable and applying Kirchhoff's law to the infinitesimal element,  $ds$ , the following current and voltage relations can be written in Laplace domain:

$$\begin{aligned} \frac{\partial}{\partial s} v(s, z) + N(z)i(s, z) &= 0 \\ \frac{\partial i(s, z)}{\partial s} + M(z)v(s, z) &= 0 \end{aligned} \quad (7)$$

where  $N(z)$  and  $M(z)$  can be defined as

$$N(z) = 2R_s, \quad M(z) = [(R_p + 2r)Cs + 1]/[R_p(1 + 2rCs)]. \quad (8)$$

Considering (7), one can obtain the following partial differential equation

$$\frac{\partial^2 v(s, z)}{\partial s^2} - K(z)v(s, z) = 0, \quad K(z) = N(z)M(z). \quad (9)$$

Taking into account the following boundary conditions for voltage and current

$$v(0, z) = V(z), \quad i(0, z) = I(z), \quad i(L, z) = 0 \quad (10)$$

the surface current  $i(s, z)$  is obtained as

$$\begin{aligned} i(s, z) &= V(z) / \sqrt{N(z)/M(z)} \left[ \tanh(\sqrt{K(z)}L) \right. \\ &\quad \times \cosh(\sqrt{K(z)}s) - \sinh(\sqrt{K(z)}s) \left. \right]. \end{aligned} \quad (11)$$

From the open-ended boundary condition  $i(L, z) = 0$ , the transfer function for impedance is concluded as

$$Z(z) = U(z)/I(z) = \sqrt{N(z)/M(z)} / \tanh(\sqrt{K(z)}L). \quad (12)$$

The ionic charge is the total ionic current passes through the polymer and density of charge, found by dividing the charge by the volume in each single unit. Following the authors method in deriving the ionic charge density [16], [19], the ionic charge density can be expressed as

$$\begin{aligned} \rho(s, z) &= M(z)V(z)g(s)/(zWh) \\ g(s) &= \cosh(\sqrt{K(z)}s) - \tanh(\sqrt{K(z)}L) \\ &\quad \times \sinh(\sqrt{K(z)}s). \end{aligned} \quad (13)$$

## B. Electromechanical Model of IPMC

This section focuses on the development of an analytical model to predict the deformation of a helical IPMC actuator subjected to an electric field. In order to obtain the dynamic equations, the naturally curved and twisted beam theory is used. There are several assumptions: 1) the IPMC actuator is isotropic and deformed within its linearly elastic range, 2) the helical IPMC is in rectangular cross section and no warping occurs during twisting deformation, 3) the cross sections of the beam do not deform in its own plane.

At the first step in calculating the strain components, we need to study the displacements field. Consider the coordinate system shown in Fig. 3. Based on the assumptions that the cross sections of the IPMC actuator do not deform in its own plane, and the actuator is so thin that  $x_n \ll 1/\kappa$  and  $x_b \ll 1/\tau$ , the displacements at every point within the cross section can be defined in terms of the displacement components  $u_t(s, t)$ ,  $u_n(s, t)$ , and  $u_b(s, t)$  of a point on the center line ( $o'$ ) along the local axes ( $\mathbf{t}, \mathbf{n}, \mathbf{b}$ ) and the position  $x_n$ ,  $x_b$ , and rotation angle  $\theta_t(s, t)$ ,  $\theta_n(s, t)$ , and  $\theta_b(s, t)$  of the cross section.

Therefore, the dynamic displacement of the helical IPMC actuator is expressed in matrix form by [41]

$$\mathbf{U} = \begin{bmatrix} 1 & 0 & 0 & 0 & x_b & -x_n \\ 0 & 1 & 0 & -x_b & 0 & 0 \\ 0 & 0 & 1 & x_n & 0 & 0 \end{bmatrix} \mathbf{p} = [\mathbf{I}_{3 \times 3} \quad \mathbf{X}_{3 \times 3}] \mathbf{p} = \mathbf{A}_U \mathbf{p} \quad (14)$$

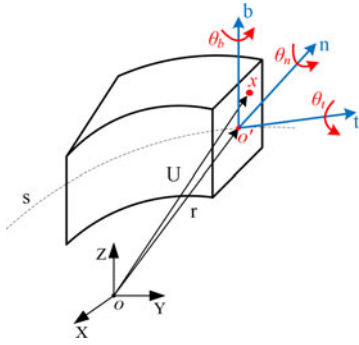


Fig. 3. Global and local frames and displacements.

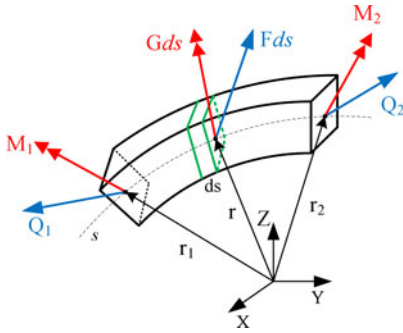


Fig. 4. Internal and applied forces.

where  $\mathbf{p}(s, t) = [\mathbf{u} \ \theta]^T = [u_t(s, t) \ u_n(s, t) \ u_b(s, t) \ \theta_t(s, t) \ \theta_n(s, t) \ \theta_b(s, t)]^T$  is the vector of the main unknown displacements.

Consider volumetric element  $ds$  of a spatially helical beam as shown in Fig. 4. Let  $\mathbf{Q}$  and  $\mathbf{M}$  be the internal force and moment vectors, respectively. Also, let the applied force and moment vectors per unit length along the curve are  $\mathbf{F}$  and  $\mathbf{G}$ , respectively. By assuming small displacements and rotations, Tabarrok and Xiong [42] derived the following translation and rotational equilibrium equations:

$$\frac{d\mathbf{Q}}{ds} + \mathbf{F} = \mathbf{0}, \quad \frac{d\mathbf{M}}{ds} + \mathbf{t} \times \mathbf{Q} + \mathbf{G} = \mathbf{0}. \quad (15)$$

Suppose that the equivalent strains related to internal forces  $\mathbf{Q}$  and  $\mathbf{M}$  are  $\varepsilon$  and  $\gamma$ , also displacement and rotation vectors related to external forces  $\mathbf{F}$  and  $\mathbf{G}$  are  $\mathbf{u}$  and  $\theta$ , respectively. By the theorem of virtual work, the following relation can be obtained:

$$\int_{s_1}^{s_2} \{ \mathbf{Q} \cdot \delta\varepsilon + \mathbf{M} \cdot \delta\gamma - \mathbf{F} \cdot \delta\mathbf{u} - \mathbf{G} \cdot \delta\theta \} ds = 0. \quad (16)$$

Substituting (15) into (16), the following relation can be obtained:

$$\int_{s_1}^{s_2} \left\{ \mathbf{Q} \cdot \delta\varepsilon + \mathbf{M} \cdot \delta\gamma + \frac{d\mathbf{Q}}{ds} \cdot \delta\mathbf{u} + \left( \frac{d\mathbf{M}}{ds} + \mathbf{t} \times \mathbf{Q} \right) \cdot \delta\theta \right\} ds = 0 \quad (17)$$

from the vector algebra, we can summarize the aforementioned equation as

$$\int_{s_1}^{s_2} \left\{ \mathbf{Q} \cdot \delta \left( \varepsilon - \frac{d\mathbf{u}}{ds} + \theta \times \mathbf{t} \right) + \mathbf{M} \cdot \delta \left( \gamma - \frac{d\theta}{ds} \right) \right\} ds + (\mathbf{Q} \cdot \delta\mathbf{u})|_{s_1}^{s_2} + (\mathbf{M} \cdot \delta\theta)|_{s_1}^{s_2} = 0. \quad (18)$$

Hence, to establish the aforementioned equation, we can obtain the following strain-displacement relations for a point on the center line of the helix ( $o'$  as shown in Fig. 3)

$$\varepsilon = \frac{d\mathbf{u}}{ds} + \mathbf{t} \times \theta = \mathbf{u}' + \mathbf{N}^T \mathbf{u} + \mathbf{t} \times \theta = \mathbf{u}' + \mathbf{N}^T \mathbf{u} + \mathbf{A}_\theta \theta$$

$$\mathbf{A}_\theta = \begin{bmatrix} 0 & 0 & 0 \\ 0 & 0 & -1 \\ 0 & 1 & 0 \end{bmatrix}, \quad \gamma = \frac{d\theta}{ds} = \theta' + \mathbf{N}^T \theta. \quad (19)$$

Considering (14) and (19), the linear strain-displacement relations for a point in the plane of the cross section (point  $x$  as shown in Fig. 3) is expressed as

$$\mathbf{e} = \begin{bmatrix} e_{tt} \\ 2e_{tn} \\ 2e_{tb} \end{bmatrix} = \begin{bmatrix} 1 & 0 & 0 \\ 0 & G_n & 0 \\ 0 & 0 & G_b \end{bmatrix} \varepsilon + \begin{bmatrix} 0 & x_b & -x_n \\ -x_b & 0 & 0 \\ x_n & 0 & 0 \end{bmatrix} \gamma = \tilde{\mathbf{G}} \varepsilon + \mathbf{X} \gamma \quad (20)$$

where  $\mathbf{e}^T = [e_{tt} \ 2e_{tn} \ 2e_{tb}]^T$  is the vector of axial and shear strain components and  $G_n$  and  $G_b$  are the shape factors depending on the beam sections [43]. Since, the helical IPMC actuator is so thin, therefore, the other strain components,  $e_{nn}$ ,  $e_{bb}$ , and  $e_{bn}$ , are small and usually negligible as compared to the quantities  $e_{tt}$ ,  $e_{tn}$ , and  $e_{tb}$ .

Nemat-Nasser *et al.* [44] showed that the stress field within the membrane is decomposed in to an elastic part denoted by  $\sigma_e$  and an eigenstress,  $e_{tn}$ , and  $\sigma^*$ , which represents the effect of the imbalanced charge density. The physical interpretation of the eigenstress will be osmotic stress, electrostatic stress, cluster imbalance, and Maxwell stress tensor. For simplicity, the eigenstress is supposed to be equal electrostatic stress due to the imbalanced density. The eigenstress induced by other effects is assumed to be negligible.

$$\sigma = [\sigma_t \ 2\sigma_{tn} \ 2\sigma_{tb}]^T = \sigma_e + \sigma^* = \mathbf{Y} \varepsilon - \alpha_0 \rho(s, t) \mathbf{I} \quad (21)$$

where  $\rho(s, t)$  is the charge density,  $\alpha_0$  is the coupling constant,  $\mathbf{I}$  is the identity matrix, and  $\mathbf{Y}$  is the elastic modulus matrix.

By using the potential energy of an element, which is composed of the strain energy and the work done by the external forces, as the functional of the problem and applying the variational procedures as a mathematical tool, the resultant forces and moments on a cross section of the helical IPMC actuator are as follows:

$$Q_t = \iint \sigma_t \, dn \, db = EA (u_t' - k u_n) - \alpha_0 A \rho(s, t)$$

$$\begin{aligned}
Q_n &= \iint \sigma_m dn db = G_n GA (u'_t - \tau u_b + k u_t - \theta_b) \\
&\quad - \alpha_0 A \rho (s, t) \\
Q_b &= \iint \sigma_{tb} dn db = G_b GA (u'_b + \tau u_n + \theta_n) \\
&\quad - \alpha_0 A \rho (s, t) \\
M_t &= \iint (x_n \sigma_{tb} - x_b \sigma_m) dn db \\
&= GJ (\theta'_t - \kappa \theta_n) - \alpha_0 A (W - h) \rho (s, t) / 4 \\
M_n &= \iint x_b \sigma_t dn db = EI_n (\theta' - \tau \theta_b + k \theta_s) \\
&\quad - \alpha_0 A h \rho (s, t) / 4 \\
M_b &= - \iint x_n \sigma_t dn db = EI_b (\theta'_b + \tau \theta_n) \\
&\quad + \alpha_0 A W \rho (s, t) / 4
\end{aligned} \tag{22}$$

where  $W$  is width and  $2h$  is the thickness of the IPMC,  $A$  is the cross-sectional area,  $I_n$  and  $I_b$ , and  $J$  are the second moments of area with respect to the normal axis, binormal axis, and the torsional moment of inertia of the cross section, respectively.

We define  $\tilde{\boldsymbol{\varepsilon}}^T = [\boldsymbol{\varepsilon} \ \boldsymbol{\gamma}]$  and  $\mathbf{f}^T = [\mathbf{Q} \ \mathbf{M}] = [Q_t \ Q_n \ Q_b \ M_t \ M_n \ M_b]$  as the total strain and internal force vector. Considering (19), the matrix form of (22) can be obtained as

$$\mathbf{f} = \mathbf{D}^* \tilde{\boldsymbol{\varepsilon}} - \mathbf{A}^* \boldsymbol{\rho} (s, t), \quad \tilde{\boldsymbol{\varepsilon}} = \mathbf{p}' + \mathbf{A}_p \mathbf{p} \tag{23}$$

where

$$\begin{aligned}
\mathbf{D}_{6 \times 6}^* &= \text{diag} [EA \ G_n GA \ G_b GA \ GJ \ EI_n \ EI_b] \\
\mathbf{A}_{6 \times 1}^* &= \alpha_0 A [1 \ 1 \ 1 \ (W - h)/4 \ h/4 \ -W/4]^T \\
\mathbf{A}_p &= \begin{bmatrix} \mathbf{N}^T & \mathbf{A}_\theta \\ \mathbf{0} & \mathbf{N}^T \end{bmatrix}.
\end{aligned} \tag{24}$$

Using the Hamilton's variational principle, the following equations of motion can be obtained for a helical IPMC actuator by substituting the strain energy, kinetic energy, and virtual work into Hamilton's principle

$$\begin{aligned}
\mathbf{M} \ddot{\mathbf{p}} &= \mathbf{f}' + \mathbf{A}_f \mathbf{f} \\
\mathbf{M} &= \text{diag} [\rho A \ \rho A \ \rho A \ \rho J \ \rho I_n \ \rho I_b] \\
\mathbf{A}_f &= \begin{bmatrix} \mathbf{N}^T & \mathbf{0} \\ \mathbf{A}_\theta & \mathbf{N}^T \end{bmatrix}_{6 \times 6}.
\end{aligned} \tag{25}$$

Considering (23) and (25), the following state-space relations for the dynamics of the helical IPMC actuator is determined as a function of input voltage, physical, and geometrical constant:

$$\begin{aligned}
\frac{d\mathbf{X}(s, z)}{ds} &= \mathbf{X}'(s, z) = \tilde{\mathbf{A}} \mathbf{X}(s, z) + \tilde{\mathbf{F}}(s, z) \\
\tilde{\mathbf{A}} &= \begin{bmatrix} -\mathbf{A}_p & \mathbf{D}^{-1} \\ \mathbf{M} z^2 & \mathbf{A}_f \end{bmatrix}, \quad \tilde{\mathbf{F}} = \begin{bmatrix} \mathbf{D}^{-1} \mathbf{A}^* \boldsymbol{\rho}(s, z) \\ \mathbf{0} \end{bmatrix}
\end{aligned} \tag{26}$$

where  $\mathbf{X} = [\mathbf{p} \ \mathbf{f}]_{12 \times 1}^T$  is state vector (internal forces and displacements) of the system and  $\tilde{\mathbf{F}}(s, z)$  is the applied load. To solve the aforementioned equations, the following boundary condition is considered

$$\begin{aligned}
\text{Fixed at} \quad \beta_0 &= 0 & : \quad \mathbf{p}_0 &= \mathbf{0} \\
\text{Free at} \quad \beta_n &= 2n\pi & : \quad \mathbf{f}_n &= \mathbf{0}
\end{aligned} \tag{27}$$

where  $n$  is the number of turn of the helix.

#### IV. SOLUTIONS OF THE DIFFERENTIAL EQUATIONS

In Sections II and III, the governing equations of motion were derived for a helical IPMC actuator under applied electric field. A set of 12 nonhomogenous simultaneous differential equations with variable coefficients were shown in (26). Each one of these equations involves first-order derivatives with respect to position and input voltage. It is clear that the applied electric voltage act as a distributed external force in the right-hand side of these equations.

The transfer-matrix method is employed to analyze the dynamic response of the helical IPMC actuator in Laplace domain. The objective of this section is obtaining an incremental transfer equation that relates the state vector at two consecutive points on the curve. This finite equation is determined using the fourth-order Runge–Kutta numerical approximation [45]. The numerical expression in this manner is shown as follows:

$$\mathbf{X}(\beta_{i+1}) = \mathbf{X}(\beta_i) + (\mathbf{k}_1 + 2\mathbf{k}_2 + 2\mathbf{k}_3 + \mathbf{k}_4) \Delta\beta/6 \tag{28}$$

where

$$\begin{aligned}
\mathbf{k}_1 &= \tilde{\mathbf{A}}(\beta_i) \mathbf{X}(\beta_i) + \tilde{\mathbf{F}}(\beta_i) \\
\mathbf{k}_2 &= \tilde{\mathbf{A}}(\beta_{i+1}/2) [\mathbf{X}(\beta_i) + \mathbf{k}_1 \Delta\beta/2] + \tilde{\mathbf{F}}(\beta_{i+1}/2) \\
\mathbf{k}_3 &= \tilde{\mathbf{A}}(\beta_{i+1}/2) [\mathbf{X}(\beta_i) + \mathbf{k}_2 \Delta\beta/2] + \tilde{\mathbf{F}}(\beta_{i+1}/2) \\
\mathbf{k}_4 &= \tilde{\mathbf{A}}(\beta_{i+1}) [\mathbf{X}(\beta_i) + \mathbf{k}_3 \Delta\beta] + \tilde{\mathbf{F}}(\beta_{i+1})
\end{aligned} \tag{29}$$

by substituting (29) into (28) the following incremental transfer equation is determined:

$$\mathbf{X}(\beta_{i+1}) = \mathbf{T}_e(\beta_i) \mathbf{X}(\beta_i) + \tilde{\mathbf{F}}_e(\beta_i) \tag{30}$$

where  $\mathbf{T}_e(\beta_i)$  is the incremental transfer matrix and  $\tilde{\mathbf{F}}_e(\beta_i)$  is the load transfer vector, which can be defined as

$$\begin{aligned}
\mathbf{T}_e(\beta_i) &= \mathbf{I} + \left[ \tilde{\mathbf{A}}(\beta_{i+1}) + 4\tilde{\mathbf{A}}(\beta_{i+1}/2) + \tilde{\mathbf{A}}(\beta_i) \right] \Delta\beta/6 \\
&\quad + \left[ \tilde{\mathbf{A}}(\beta_{i+1}) \tilde{\mathbf{A}}(\beta_{i+1}/2) + \tilde{\mathbf{A}}^2(\beta_{i+1}/2) \right. \\
&\quad \left. + \tilde{\mathbf{A}}(\beta_{i+1}/2) \tilde{\mathbf{A}}(\beta_i) \right] \Delta\beta^2/6 \\
&\quad + \left[ \tilde{\mathbf{A}}(\beta_{i+1}) \tilde{\mathbf{A}}^2(\beta_{i+1}/2) + \tilde{\mathbf{A}}^2(\beta_{i+1}/2) \tilde{\mathbf{A}}(\beta_i) \right] \Delta\beta^3/12 \\
&\quad + \left[ \tilde{\mathbf{A}}(\beta_{i+1}) \tilde{\mathbf{A}}^2(\beta_{i+1}/2) \tilde{\mathbf{A}}(\beta_i) \right] \Delta\beta^4/24 \\
\tilde{\mathbf{F}}_e(\beta_i) &= \left[ \tilde{\mathbf{F}}(\beta_{i+1}) + 4\tilde{\mathbf{F}}(\beta_{i+1}/2) + \tilde{\mathbf{F}}(\beta_i) \right] \Delta\beta/6 \\
&\quad + \left[ \tilde{\mathbf{A}}(\beta_{i+1}) \tilde{\mathbf{F}}(\beta_{i+1}/2) + \tilde{\mathbf{A}}(\beta_{i+1}/2) \tilde{\mathbf{F}}(\beta_{i+1}/2) \right. \\
&\quad \left. + \tilde{\mathbf{A}}(\beta_{i+1}/2) \tilde{\mathbf{F}}(\beta_i) \right] \Delta\beta^2/6
\end{aligned} \tag{31}$$

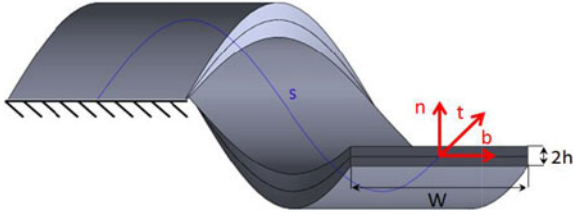


Fig. 5. Equivalent helical bimorph model.

$$\begin{aligned}
& + \tilde{\mathbf{A}}(\beta_{i+1}/2) \tilde{\mathbf{F}}(\beta_i) \Delta \beta^2 / 6 \\
& + \left[ \tilde{\mathbf{A}}(\beta_{i+1}) \tilde{\mathbf{A}}(\beta_{i+1}/2) \tilde{\mathbf{F}}(\beta_{i+1}/2) \right. \\
& + \tilde{\mathbf{A}}^2(\beta_{i+1}/2) \tilde{\mathbf{F}}(\beta_i) \Delta \beta^3 / 12 \\
& \left. + \left[ \tilde{\mathbf{A}}(\beta_{i+1}) \tilde{\mathbf{A}}^2(\beta_{i+1}/2) \tilde{\mathbf{F}}(\beta_i) \right] \Delta \beta^4 / 24. \right. \quad (32)
\end{aligned}$$

For the free vibration case, the applied load vector,  $\tilde{\mathbf{F}}(s, z)$ , is equal to zero and the Laplace parameter  $z$  is replaced with  $i\omega$ . The eigenvalues in this case give the natural frequencies. Considering (30) in homogenous form and the clamped-free boundary condition, (27), the following relation between the initial and end state vectors is obtained as

$$\begin{aligned}
\mathbf{X}(\beta_n) &= \mathbf{TX}(\beta_0) \\
\begin{bmatrix} \mathbf{p}_n \\ \mathbf{f}_n \end{bmatrix} &= \begin{bmatrix} \mathbf{T}_{11} & \mathbf{T}_{12} \\ \mathbf{T}_{21} & \mathbf{T}_{22} \end{bmatrix} \begin{bmatrix} \mathbf{p}_0 \\ \mathbf{f}_0 \end{bmatrix} \rightarrow \begin{bmatrix} \mathbf{p}_n \\ \mathbf{0} \end{bmatrix} \\
&= \begin{bmatrix} \mathbf{T}_{11} & \mathbf{T}_{12} \\ \mathbf{T}_{21} & \mathbf{T}_{22} \end{bmatrix} \begin{bmatrix} \mathbf{0} \\ \mathbf{f}_0 \end{bmatrix} \quad (33)
\end{aligned}$$

where  $\mathbf{T}$  is the overall transfer matrix. As shown in (33), we can relate the six zero entries of  $\mathbf{X}(\beta_n)$  to the six nonzero elements of  $\mathbf{X}(\beta_0)$ . Therefore, the following reduced overall transfer matrix is given by

$$\mathbf{T}_{22} \mathbf{f}_0 = \mathbf{0}. \quad (34)$$

For nontrivial solutions, the determinant of  $\mathbf{T}_{22}$  must be zero. The natural frequencies of the helical IPMC are those that satisfy this requirement and determined using Müller's method [46]. Once a natural frequency is determined, the corresponding matrix  $\mathbf{T}_{22}$  evaluated at this frequency. The six nonzero elements of the initial state vector,  $\mathbf{f}_0$ , are the eigenvector corresponding to the one eigenvalue very close to zero of the matrix  $\mathbf{T}_{22}$ . By using  $\mathbf{f}_0$  and considering the homogenous form of (30), the mode shape for any natural frequency can be easily computed evolve the state vector  $\mathbf{X}$  along the helical actuator using the element transfer matrices.

## V. MODELING WITH A COMMERCIAL FE PACKAGE

In this section, we utilize the equivalent bimorph beam model presented by Lee *et al.* [47] to predict the performance of an IPMC actuator. Because of the helical structure of the IPMC actuator, the helical bimorph beam model is newly developed

TABLE I  
PHYSICAL AND PIEZOELECTRIC PROPERTIES OF THE IPMC ACTUATOR

Piezoelectric Parameters	$d_{31}$	$d_{32}$		
	1.8e-8	1.8e-8		
IPMC Parameter[29]	$\nu$	E (GPa)	$\epsilon$ (Fm <sup>-1</sup> )	$\rho$ (kg m <sup>-3</sup> )
	0.487	0.5	0.031	2600

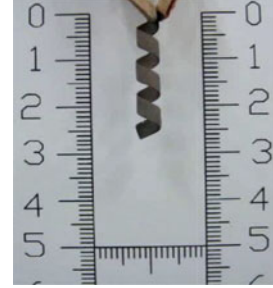


Fig. 6. Fabricated helical IPMC actuator.

TABLE II  
VALUES OF ELECTRICAL PARAMETERS [16], [19]

Parameters	$R_s$ [ $\Omega$ /cm]	$R$ [ $\Omega \cdot$ cm]	$R_p$ [ $\Omega \cdot$ cm]	$C$ [F/cm]
Value	22.5	12.43	24645	0.0019

for obtaining the electromechanical coupling coefficient, which can be considered as equivalent material parameter for the finite-element analyses [47], [48].

The geometry of the proposed helical IPMC actuator is simply modeled by using the 3-D modeling software package. The equivalent helical bimorph beam model, shown in Fig. 5, assumes that the IPMC having two helical layers of the same thickness (each is half the thickness of the actuator). The material properties of the helical IPMC actuator are given in Table I.

## VI. EXPERIMENTS AND ANALYSIS

Nafion-based IPMC actuators with platinum (Pt) electrode layers were used in this experiment. An IPMC was fabricated with Nafion (N-117, DuPont) through an electroless plating process [1]. The helical IPMC actuators were fabricated as mentioned earlier by Li *et al.* [31]. The IPMC was cut into strips, which have the designed length and width. Afterward, the strips were helically coiled on glass rods and dipped into distilled water at 90 °C for 1 h to fix the helix shape by the thermal treatment. For more information about the fabrication process, refer to [31]. The fabricated helical IPMC actuator is shown in Fig. 6. The impedance analyzer (VersaSTAT3-model 616A) was used for measuring the complex impedance of the IPMC. To measure the electromechanical responses of the actuator, a laser displacement sensor (Keyence, LK-031), a current amplifier (UPM1503), and an NI-PXI 8110 data acquisition system were used.

TABLE III  
DIFFERENT MODEL OF THE HELICAL IPMC ACTUATOR [25]

Name	Width (mm)	Pitch (mm)	Diameter (mm)
3D3P3W	3	3	3
5D3P3W	3	3	5
3D3P5W	5	3	3
3D5P5W	5	5	3
5D5P5W	5	5	5

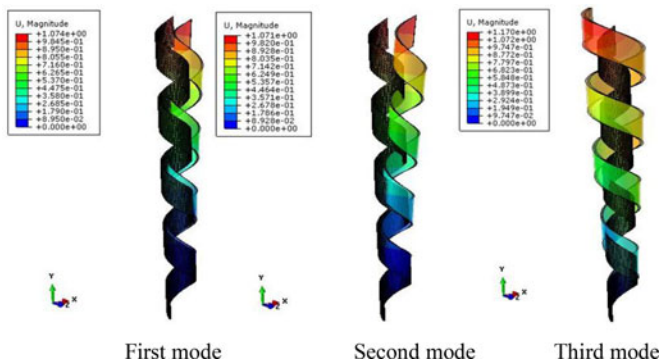


Fig. 7. First three mode shapes of the helical IPMC actuator. (Captured from FE Package).

## VII. MODEL VERIFICATION

In order to validate the values of electrical parameters from the impedance model presented here, (12), experimental results were captured from the impedance analyzer. The nonlinear least-square method was used to find the optimum parameter  $x^*$  that minimizes the squared error between the empirical impedance response and the theoretical model. Therefore, we utilize the electrical parameters as listed in Table II and also the experimental results of a helical IPMC actuator [16], [19], [31]. To investigate the effect of the geometrical parameters of the helical IPMC actuator on the dynamic responses and for comparing with experimental results [31], we use five different models as listed in Table III.

Some numerical results are given to validate the analytical expressions obtained in the preceding section, which will be directly applied to compute the natural frequencies and the corresponding mode shapes of a cylindrical helical actuator with a rectangular cross section. Therefore, a general-purpose computer program is coded to perform the free vibration analysis of the helical actuator. The other geometrical and physical parameters  $n = 4.367$  (number of turn of the helix),  $h = 0.11$  mm,  $\alpha = 1.1384^\circ$ ,  $\alpha_0 = 0.102$  and shape factors  $G_n = G_b = 0.8567$  [43] are considered.

The first three mode shapes of the helical IPMC actuator are captured from the FE Package and MATLAB software and results are shown in Figs. 7 and 8, respectively. As can be seen, the first and second modes are predominantly bending motion and third mode is predominantly torsional. Since the helical IPMC actuator is a multi-DOF actuator and as regards the bending modes, torsional modes, and longitudinal modes are excited at the specific frequencies, therefore, the natural frequencies of the helical IPMC actuators play an important

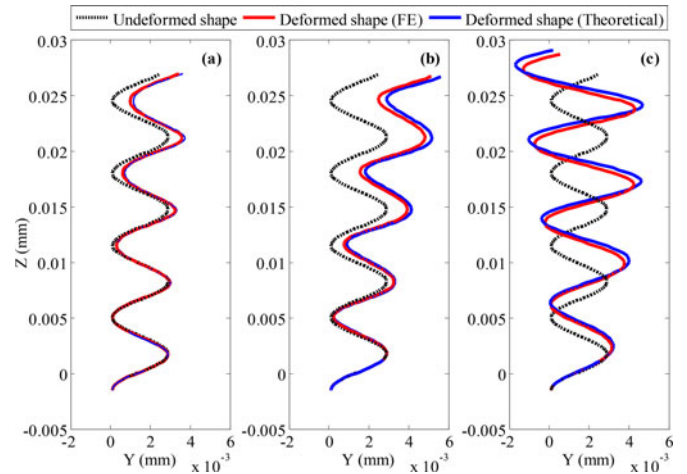


Fig. 8. First three mode shapes of the free vibrating cylindrical helical actuator: (a) first mode (b) second mode (c) third mode. (Captured from MATLAB software).

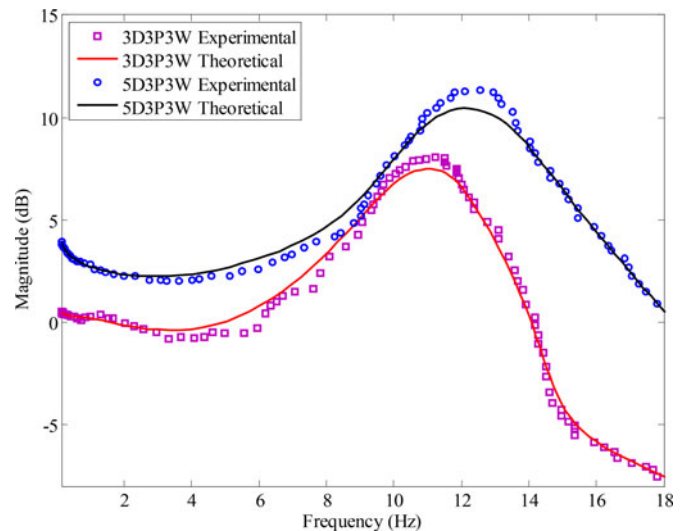


Fig. 9. Comparison of the proposed actuation response of the 3D3P3W and 5D3P3W model with the experimental data.

TABLE IV  
FIRST FOUR NATURAL FREQUENCIES (IN Hz)

Mode Number	FE Package	Present Study	Experiment
1	13.52	13.3892	13.29
2	15.386	15.1	–
3	61.516	60.634	–
4	84.456	83.056	–

role in modal analysis. The actuation model is next verified by applying sinusoidal actuation signals,  $V(t)$ , with amplitude of 0.1 V and frequencies ranging from 0.01 to 100 Hz. Fig. 9 compares our proposed actuation model with the experimental results for two helical IPMC actuators with different diameters [31]. As can be seen, our proposed dynamic model closely approximates the experimental data. It is clear that the 3D3P3W actuator has lower natural frequency and magnitude in the whole

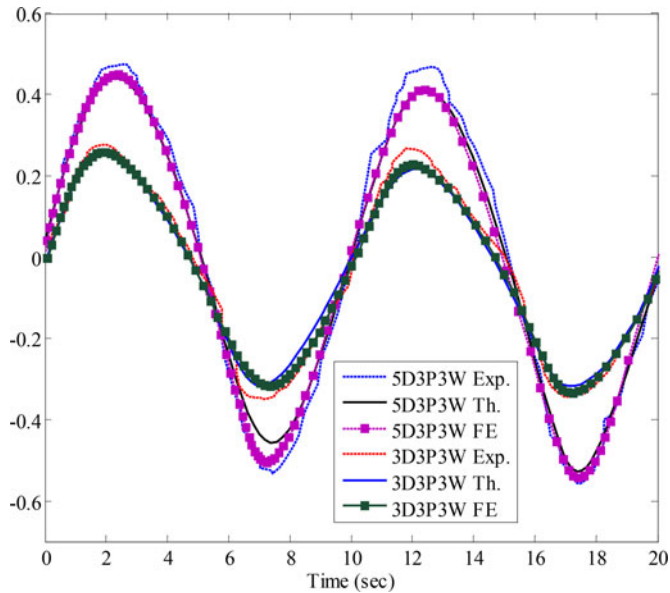


Fig. 10. Comparison of the radial displacements of the helical IPMC actuators with different diameters (Exp.: experiment, Th.: theoretical, FE: FE package).

excitation frequency range in comparison with the 5D3P3W actuator.

The first four natural frequencies obtained by the program prepared in this study for 5D3P3W model, together with those obtained from commercial FE package and experimental data are given in Table IV. As can be observed from the Table IV, it is clearly evident that the results of the present model demonstrate a good agreement with those of FE package and experiments.

To investigate the performance of the helical IPMC actuator under different structural parameters, the harmonic responses subject to an electrical input potential with peak voltage of 2 V and frequency of 0.1 Hz are performed. Fig. 10 shows the harmonic responses of the helical IPMC actuator with different diameter. It is evident that the helical IPMC actuator with 5-mm diameter shows much larger radial displacement than that with 3-mm diameter and also as illustrated in Fig. 10, the behavior of the proposed model is similar to the experimental and commercial FE package results.

## VIII. CONCLUSION

In this study, we report an innovative dynamic model of the helical IPMC actuator to accurately compute time responses and deformed shapes under various electrical input signals. To the best of authors' knowledge, it is the first time that an analytical expression was derived for the computation of mode shapes and dynamic responses of a helical IPMC actuator with fixed-free ends. First, curvilinear coordinate and intrinsic equations of a naturally curved and twisted beam are used to formulate an electromechanical model based on the distributed *RC* line model. Next, a numerical transfer-matrix method was used to solve a system of 12 linear ordinary differential equations with boundary conditions. An incremental transfer function was obtained by applying a fourth-order Runge–Kutta method. The effect of the structural shape parameters on the performance of the helical IPMC actuator was also analyzed using the analytical model. Analytical solution was compared with the experimen-

tal data as well as results of a commercial FE package. It is shown that the three results closely follow each other indicating validity of the proposed model. Additionally, the findings indicate that the diameter, among the structural parameters, plays a key role in the actuation performance of the helical actuator. The analytical model is general and can accommodate cylindrical or noncylindrical helical IPMC actuators with different cross-sectional shapes as well as various end conditions.

The contributions of this paper are summarized as 1) presenting a simple distributed electrical model that can replace the complicated physical model based on ionic motion, 2) determining an analytical function for the charge density, 3) developing an analytical expression for dynamic responses of the helical IPMC actuator based on the naturally curved and twisted beam theory, 4) investigating the effect of the structural parameters on the actuation performance of the helical IPMC actuator, and 5) modeling the helical IPMC actuator in a commercial FEM software.

## REFERENCES

- [1] M. Shahinpoor and K. J. Kim, "Ionic polymer-metal composites: I. Fundamentals," *Smart Mater. Struct.*, vol. 10, pp. 819–833, 2001.
- [2] M. Shahinpoor, Y. Bar-Cohen, J. O. Simpson, and J. Smith, "Ionic polymer-metal composites (IPMCs) as biomimetic sensors, actuators and artificial muscles—a review," *Smart Mater. Struct.*, vol. 7, pp. R15–R30, 1999.
- [3] S. W. Yeom and I. K. Oh, "A biomimetic jellyfish robot based on ionic polymer metal composite actuators," *Smart Mater. Struct.*, vol. 18, pp. 085002-1–085002-10, 2009.
- [4] S. Guo, T. Fukuda, and K. Asaka, "A new type of fish-like underwater microrobot," *IEEE/ASME Trans. Mechatron.*, vol. 8, no. 1, pp. 136–141, Mar. 2003.
- [5] B. Kim, J. Ryu, Y. Jeong, Y. Tak, B. Kim, and J. Park, "A ciliary based 8-legged walking micro robot using cast IPMC actuators," in *Proc. IEEE Int. Conf. Robot.*, 2003, vol. 3, pp. 2940–2945.
- [6] M. Yamakita, N. Kamamichi, T. Kozuki, K. Asaka, and L. Zhi-Wei, "A snake-like swimming robot using IPMC actuator and verification of doping effect," *IEEE/RSJ Int. Conf. Intel. Robots Syst.*, 2005, pp. 2035–2040.
- [7] M. Shahinpoor and K. J. Kim, "Ionic polymer-metal composites: IV. Industrial and medical applications," *Smart Mater. Struct.*, vol. 14, pp. 197–214, 2005.
- [8] G. H. Feng and J. W. Tsai, "Micromachined optical fiber enclosed 4-electrode IPMC actuator with multidirectional control ability for biomedical application," *Biomed. Microdevices*, vol. 13, no. 1, pp. 169–177, 2011.
- [9] R. Tiwari and K. J. Kim, "IPMC as a mechanoelectric energy harvester: Tailored properties," *Smart Mater. Struct.*, vol. 22, no. 1, pp. 015017-1–015017-16, 2013.
- [10] R. Tiwari and K. Kim, "Disc-shaped ionic polymer metal composites for use in mechano-electrical applications," *Smart Mater. Struct.*, vol. 19, no. 6, pp. 065016-1–065016-7, 2010.
- [11] Y. Cha, C. N. Phan, and M. Porfiri, "Energy exchange during slamming impact of an ionic polymer metal composite," *Appl. Phys. Lett.* vol. 101, no. 9, 094103-1–094103-4, 2012.
- [12] Y. Cha, L. Shen, and M. Porfiri, "Energy harvesting from underwater torsional vibrations of a patterned ionic polymer metal composite," *Smart Mater. Struct.*, vol. 22, no. 5, pp. 055027-1–055027-13, 2013.
- [13] Y. Cha, M. Verotti, H. Walcott, S. D. Peterson, and M. Porfiri, "Energy harvesting from the tail beating of a carangiform swimmer using ionic polymer metal composites," *Bioinspir. Biomim.*, vol. 8, no. 3, 036003-1–036003-15, 2013.
- [14] K. J. Kim and M. Shahinpoor, "Ionic polymer-metal composites: II. Manufacturing techniques," *Smart Mater. Struct.*, vol. 12, no. 1, pp. 65–79, 2003.
- [15] J. H. Jeon, S. W. Yeom, and I. K. Oh, "Fabrication and actuation of ionic polymer metal composites patterned by combining electroplating with electroless plating," *Composites Part A*, vol. 39, no. 4, pp. 588–596, 2008.
- [16] H. Moeinkhah, J. Rezaeepazhand, and A. Akbarzadeh, "Analytical dynamic modeling of a cantilever IPMC actuator based on a distributed electrical circuit," *Smart Mater. Struct.*, vol. 22, no. 5, pp. 055033-1–055033-10, 2013.



- [17] Y. Cha and M. Porfiri, "Bias-dependent model of the electrical impedance of ionic polymer-metal composites," *Phys. Rev. E*, vol. 87, no. 2, pp. 022403-1–022403-16, 2013.
- [18] M. Porfiri, "Charge dynamics in ionic polymer metal composites," *J. Appl. Phys.*, vol. 104, no. 10, pp. 104915-1–104915-10, 2008.
- [19] H. Moeinkhah, J. Y. Jung, J. H. Jeon, A. Akbarzadeh, J. Rezaeepazhand, K. C. Park, and I. K. Oh, "How does clamping pressure influence actuation performance of soft ionic polymer-metal composites?," *Smart Mater. Struct.*, vol. 22, no. 2, pp. 025014-1–025014-11, 2013.
- [20] M. Porfiri, "Influence of electrode surface roughness and steric effects on the nonlinear electromechanical behavior of ionic polymer metal composites," *Phys. Rev. E*, vol. 79, no. 4, pp. 0415031-1–0415031-13, 2009.
- [21] P. Nardinocchi and M. Pezzulla, "Curled actuated shapes of ionic polymer metal composites strips," *J. Appl. Phys.*, vol. 113, no. 22, pp. 224906-1–224906-8, 2013.
- [22] S. Galante, A. Lucantonio, and P. Nardinocchi, "The multiplicative decomposition of the deformation gradient in the multiphysics modeling of ionic polymer gels," *Int. J. Nonlinear Mech.*, vol. 51, pp. 112-120, 2013.
- [23] Z. Chen and X. Tan, "A control-oriented and physics-based model for ionic polymer-metal composite actuators," *IEEE/ASME Trans. Mechatron.*, vol. 13, no. 5, pp. 519-529, Oct. 2008.
- [24] D. Liu, A. J. McDaid, K. C. Aw, and S. Q. Xie, "Position control of an ionic polymer metal composite actuated rotary joint using iterative feedback tuning," *Mechatronics*, vol. 21, no. 1, pp. 315-328, 2011.
- [25] H. Moeinkhah, A. Akbarzadeh, and J. Rezaeepazhand, "Design of a robust QFT position controller for an IPMC actuator using an analytical dynamic model," *J. Intell. Mater. Syst. Struct.*, Doi:10.1177/1045389X13512906, in press.
- [26] A. A. Lucas and P. Lambin, "Diffraction by DNA, carbon nanotubes and other helical nanostructures," *Rep. Prog. Phys.*, vol. 68, no. 5, pp. 1181-1249, 2005.
- [27] A. T. ALI, "Position vectors of general helices in Euclidean 3-space," *Bull. Math. Anal. Appl.*, vol. 3, no. 2, pp. 198-205, 2010.
- [28] I. Spinella, E. Dragoni, and F. Stortiero, "Modeling, prototyping, and testing of helical shape memory compression springs with hollow cross section," *J. Mech. Des.*, vol. 132, pp. 061008-1–061008-9, 2010.
- [29] H. Han, K. K. Angb, Q. Wangc and F. Taheri, "Buckling enhancement of epoxy columns using embedded shape memory alloy spring actuators," *Compos. Struct.*, vol. 72, no. 2, pp. 200-211, 2006.
- [30] H. J. Lee and J. J. Lee, "Evaluation of the characteristics of a shape memory alloy spring actuator," *Smart Mater. Struct.*, vol. 9, no. 6, pp. 817-823, 2000.
- [31] S. L. Li, W. Y. Kim, T. H. Cheng, and I. K. Oh, "A helical ionic polymer-metal composite actuator for radius control of biomedical active stents," *Smart Mater. Struct.*, vol. 20, no. 3, pp. 035008-1–035008-8, 2011.
- [32] M. Shahinpoor, K. J. Kim, and M. Mojarad, *Artificial Muscles: Applications of Advanced Polymeric Nanocomposites*. New York, NY, USA: Taylor & Francis, 2007.
- [33] K. Washizu, "Some consideration on a naturally curved and twisted slender beam," *J. Math. Phys.*, vol. 43, no. 2, pp. 111-116, 1964.
- [34] Y. Cha, M. Aureli, and M. Porfiri, "A physics-based model of the electrical impedance of ionic polymer metal composites," *J. Appl. Phys.* vol. 111, no. 2, 124901-1–124901-14, 2012.
- [35] T. Wallmersperger, D. J. Leo, and C. S. Kothera, "Transport modeling in ionomeric polymer transducers and its relationship to electromechanical coupling," *J. Appl. Phys.*, Vol. 101, pp. 024912-1–024912-9, 2007.
- [36] T. Wallmersperger, B. J. Akle, D. J. Leo, and B. Kröplin, "Electromechanical response in ionic polymer transducers: An experimental and theoretical study," *Compos. Sci. Technol.*, vol. 68, no. 5, pp. 1173-1180, 2008.
- [37] Z. Chen, D. R. Hedgepeth, and X. Tan, "A nonlinear, control-oriented model for ionic polymer metal composite actuators," *Smart Mater. Struct.*, vol. 8, no. 5, pp. 055008-1–055008-9, 2009.
- [38] M. Vahabi *et al.*, "Experimental identification of IPMC actuator parameters through incorporation of linear and nonlinear least squares methods," *Sens. Actuators A*, vol. 168, pp. 140-148, 2011.
- [39] X. Bao, Y. Bar-Cohen, and S. S. Lih, "Measurements and macro models of ionomeric polymer-metal composites (IMPC)," in *Proc. SPIE EAPAD Conf.*, 2002, pp. 286-293.
- [40] Y. Cha, F. Cellini, and M. Porfiri, "Electrical impedance controls mechanical sensing in ionic polymer metal composites," *Phys. Rev. E*, vol. 88, no. 6, p. 062603, 2013.
- [41] V. V. Novozhilov, *Foundation of the Nonlinear Theory of Elasticity*. New York, NY, USA: Graylock Press, 1963.
- [42] B. Tabarrok and Y. Xiong, "On the buckling equations for spatial rods," *Int. J. Mech. Sci.*, vol. 31, no. 3, pp. 179-192, 1989.
- [43] L. Brancheriau, "Influence of cross section dimensions on Timoshenko's shear factor application to wooden beams in free-free flexural vibration," *Ann. For. Sci.*, vol. 63, pp. 319-321, 2006.
- [44] S. Nemat-Nasser and J. Y. Li, "Electromechanical response of ionic polymer-metal composites," *J. Appl. Phys.*, vol. 87, no. 7, pp. 3321-3331, 2000.
- [45] E. C. Pestel and F. A. Leckie, *Matrix Methods in Elastomechanics*. vol. 51213, New York, NY, USA: McGraw-Hill, 1963.
- [46] D. Pearson, "The transfer matrix method for the vibration of compressed helical springs," *J. Mech. Eng. Sci.*, vol. 24, no. 4, pp. 163-171, 1982.
- [47] S. Lee, H. C. Park, and K. J. Kim, "Equivalent modeling for ionic polymer-metal composite actuators based on beam theories," *Smart Mater. Struct.*, vol. 14, no. 6, pp. 1363-1368, 2005.
- [48] H. D. Çilingir and M. Papila, "Equivalent electromechanical coefficient for IPMC actuator design based on equivalent bimorph beam theory," *Exp. Mech.*, vol. 50, no. 8, pp. 1157-1168, 2010.



**Hossein Moeinkhah** received the B.S. and Ph.D. degrees both in mechanical engineering from the Ferdowsi University of Mashhad, Mashhad, Iran, in 2004 and 2014, respectively, and the M.S. degree in mechanical engineering from the Isfahan University of Technology, Isfahan, Iran, in 2006.

He joined the University of Sistan and Baluchestan, Zahedan, Iran, in 2014, where he is currently an Assistance Professor in the Mechanical Engineering Department. His research interests include electroactive polymer actuators and sensors, biomedical active device, and robotics and control.



**Jalil Rezaeepazhand** received the B.S. degree in mechanical engineering from the Ferdowsi University of Mashhad (FUM), Mashhad, Iran, in 1988, and the Master and Ph.D. degree both in aerospace engineering from the University of Cincinnati, Cincinnati, OH, USA, in 1992 and 1995, respectively.

He joined the Department of Mechanical Engineering, FUM, in 1996, where he is currently a Professor of aerostructures. His research interests include structural stability, smart structures, and structural similitude and scaling for laminated composites.



**Alireza Akbarzadeh** received the Ph.D. degree in mechanical engineering in 1997 from the University of New Mexico, Albuquerque, NM, USA.

He worked at Motorola, USA, for 15 years, where he led R&D as well as automation teams. He joined the Ferdowsi University of Mashhad, Mashhad, Iran, in 2005, and is currently a full Professor in the Mechanical Engineering Department. He has more than 50 journal publications and more than 65 conference papers. His research interests include robotics (parallel robots, biologically inspired robots, bipedal

robots, and rehabilitation robotics), dynamics, kinematics, control, automation, optimization as well as design and analysis of experiments. He is also a Founding Member of the Center of Excellence on Soft Computing and Intelligent Information Processing, FUM.



**Il-Kwon Oh** received the B.S. degree in aerospace engineering from Inha University, Incheon, Korea, in 1995, and the M.S. degree in aerospace engineering and the Ph.D. degree in mechanical engineering from the Korea Advanced Institute of Science and Technology (KAIST), Daejeon, Korea, in 1997, and 2001, respectively.

In 2010, he became an Associate Professor in the School of Mechanical, Aerospace and Systems Engineering, KAIST, where he is the Director of the Structural Dynamics and Smart Systems Laboratory.

His research interests include electroactive polymers, biomedical active devices, vibration and noise control, and smart materials and systems.